ELSEVIER

Journal of Power Sources 91 (2000) 177–192

JOURNAL OF POWER SOURCES

www.elsevier.com/locate/jpowsour

Structural changes of active materials and failure mode of a valve-regulated lead-acid battery in rapid-charge and conventional-charge cycling

T.G. Chang *, D.M. Jochim

Cominco Ltd., Product Technology Centre, Mississauga, Ontario, Canada L5K 1B4

Received 14 December 1999; accepted 4 March 2000

Abstract

Spirally wound 12-V valve-regulated lead-acid batteries were subjected to conventional-charge and rapid-charge cycling tests. The cycle life was 250 cycles for the conventional-charge regime and 1000 cycles for the rapid-charge regime. In conventional-charge cycling, the positive active material quickly expanded and developed a coralloid structure in association with lowered utilisation and integrity. In rapid-charge cycling, no coralloid structure developed and the expansion was smaller and much slower. Correspondingly, the particle size of the negative active material grew in both cycling tests, but at a much slower rate in rapid-charge cycling. With the expansion of the positive active material, the negative active material was compressed. In the failed batteries, about one-third of the negative active material in the centre of the electrode was compressed almost into a solid non-porous mass. This densification process also occurred at a much slower rate in rapid-charge cycling. At the point of failure, the discharge capacity of all test batteries was limited by the negative electrode, although it was limited by the positive electrode at the beginning of the cycling tests. The cause of failure for most of the batteries, regardless of the charging regime, was the occurrence of "soak-through" shorts caused by numerous minute lead dendrites formed in the separator. This might have been encouraged by the formation of shorter distances between the two electrodes, created by the compression of the separator as a result of the expansion of the positive active material.

Keywords: Lead-acid batteries; Active material structure; Charging regime; Cycle life

1. Introduction

The ampere-hour rule has been accepted as a rule of thumb since 1935 [1–4]. It states that "A battery can accept as much current (in amperes) as it needs in capacity (in ampere hours) until it reaches full charge" [3]. However, since 1991, it has been shown that lead-acid batteries can accept a current much higher than that dictated by the ampere–hour rule with neither apparent detrimental effect on the batteries, nor excessive waste of charging energy [5–10]. This means that the daily travel range and working hours of lead-acid battery-powered vehicles and devices can be extended by rapid recharges.

It is anticipated that rapid recharges will affect the structure of the active material. However, it has not yet been clearly shown whether the effects of rapid recharges are detrimental or beneficial to lead-acid batteries.

2. Experimental

The test batteries were spirally wound 12-V 52 A h Optima prototype deep cycling batteries, produced by Optima Advanced Technology, Aurora, CO, USA. The batteries each weighed 20.1 to 20.7 kg upon receipt. Their initial internal resistance (charged), as measured by a Hewlett Packard A.C. milliohm meter (Model 4328A), was 2.5 to 2.7 mΩ. The grids were punched cast lead sheet, and the composition for both positive and negative grids was Pb-0.6% Sn.

* Corresponding author. Tel.: +1-905-822-2022; fax: +1-905-822-2882.

0378-7753/00/$ - see front matter
PII: S0378-7753(00)00470-5

2.1. Cycling test systems

2.1.1. Rapid-charge cycling test system

MinitChargers™ (Model MC6-300A), manufactured by Norvik Technologies, Mississauga, ON, Canada, were used for charging; they charged batteries with a constant resistance-free voltage limit [11–15]. Every 100 milliseconds, the charger interrupted the current, measured the resistance-free battery voltage, and adjusted the current to maintain the constant resistance-free voltage set by the operator. The applied voltage was also adjusted to compensate for deviations from 25°C of the measured temperature on the side wall of the battery. During a discharge, current from the test battery was drawn by an electronic load. The test systems were controlled and monitored by a PC computer with analog and digital I/O boards. The computer program used for the system was developed using Viewdac™ software (Asyst Software Technologies, Rochester, NY, USA).

2.1.2. Conventional-charge cycling test system

This system could test three batteries simultaneously. During a charge period, the test batteries were connected in parallel and charged with a voltage and current-controlled power supply. During a discharge period, the test batteries were serially connected. The test was monitored and controlled by a PC computer with I/O boards in the computer and a program written on a platform using an INTEL iRMX real-time operating system.

2.2. Test procedure

All batteries were first subjected to five pre-test conditioning cycles. In these cycles, the batteries were charged at a constant voltage limit of 16.5 V, with a maximum current limit of 10 A, for 10 h. The charging voltage was adjusted, if necessary, to ensure that at the end of charging at least 120% of the previous discharge was returned. The batteries were discharged at 24.7 A, a 2-h rate, to 10.5 V (100% DOD). The following cycling tests were conducted at ambient temperature and no special means were used for cooling the test batteries. However, the ambient temperature was monitored throughout the test.

2.2.1. Conventional-charge life-cycle test

2.2.1.1. Charging regime. A constant voltage charge for 10 h with a current limit of about 10 A was used. The voltage was selected such that after 10 h of charging the charge returned was 110% to 115%. Thus, the charging voltage and, at times, the charging time had to be judiciously adjusted during the test of a battery. However, the end-of-charge (EOC) voltage was not allowed to be less than 14.1 V.

2.2.1.2. Discharge regime. The test battery was discharged at 24.7 A to 11.6 V which corresponded to a DOD of 80%. Every 50 cycles, the battery was discharged to 10.5 V (100% DOD) for three cycles.

2.2.1.3. Rest period. After each charge and discharge period, there was a 15-min rest.

2.2.2. Rapid-charge life-cycle test

Two charging regimes were used in the cycling.

2.2.2.1. Partial charge. The test batteries were charged for 15 min at a fixed resistance-free voltage with a current limit of 250 A, such that the charge returned after 5 and 15 min would be equivalent to 50% and 80%, respectively, of the ampere–hours delivered by the test battery when discharged to 11.6 V (DOD of 80%).

2.2.2.2. Full charge. A two-step charge was used. In the first step, the battery was charged at the same resistance-free voltage limit used in the partial-charge regime with a current limit of 100 A for 1 h. Then, the charging entered the second step which lasted 3 h. The voltage in this period was adjusted to a level such that at the end of the charging period 110% to 120% of the previous discharge was returned.

2.2.2.3. Discharge regime. The test battery was discharged at 24.7 A to 11.6 V which corresponded to 80% DOD.

2.2.2.4. Rest period. After each charge and discharge, the battery was allowed to rest for 15 min.

2.2.2.5. Cycling sequence. For five consecutive cycles, the battery was only partially charged and then it was fully charged for one cycle. This pattern was repeated until the end of the test. Every 50 cycles, the test battery was capacity-discharged (100% DOD) and fully recharged for three consecutive cycles to determine its capacity at that time.

2.3. Physico-chemical characterisation of the electrodes in the test batteries

The test batteries were stopped at various stages of cycling and subjected to the tests and assays described below.

2.3.1. Morphological study

Active materials taken from the test batteries were mounted in polyester resin and examined by optical microscopes and a JEOL (Model JSM-5800LV) scanning electron microscope (JEOL, Tokyo, Japan). The scanning electron microscope had a PGT IMIX-PTS energy dispersive

X-ray spectrometer (Princeton Gamma-Tech, Princeton, NJ, USA) which could perform elementary analysis of the samples.

2.3.2. Surface area and pore-size distribution

Samples were taken from various locations in the electrode strips for both positive and negative electrodes, and their surface areas and pore-size distributions were determined. The analyser was a Micromeritics ASAP 2010 (Micromeritics Instrument, Norcross, GA, USA). Nitrogen was the adsorbate for the positive active material and krypton for the negative active material. A multiple-point BET method was used for the surface area determination. For the positive active material, a BJH (Barrett, Johner and Halenda) method [16,17] was used to determine the pore-size distribution by analysing the desorption branch of the isotherm. In the calculation, the pores are assumed to be cylindrical in shape, and the cores of the pores are defined by the Kelvin equation [17].

2.3.3. X-ray diffractometric analysis

The X-ray diffractometer was equipped with a Philips (Model PW11/00) 1000 W generator and a wide-angle goniometer (Philips PW1050/25) with a graphite monochromater (AMR model 3-202). Variation of the α-PbO_2/β-PbO_2 ratio with cycling was determined using intensity data from the recorded diffraction patterns. Crystallite size and strain were calculated from the line-width data [18–27].

2.3.4. Lead dioxide contents

A standard thiosulfate iodide method [28] was used to determine the lead dioxide content in the positive active material.

2.3.5. Metallic lead contents

A mannitol solution method [29] was used to determine the metallic content in the negative active material.

2.3.6. Sulfuric acid concentration

Three pieces of the separator of a cell from a disassembled battery were removed from the upper, middle and lower parts of the separator strip, respectively. The acid in each piece of the separator was extracted and titrated to determine the concentration of acid in the separator.

3. Results

3.1. Cycle life

3.1.1. Conventional-charge cycling

As shown in Table 1, four batteries were removed from the test before failure and three were cycled to failure. The average cycle life was 255 cycles with a total accumulated discharge output of 9700 A h and a total charge to discharge ampere–hours ratio of 1.17. Fig. 1 shows the amounts of charge and discharge in ampere–hours in each cycle for one of the failed batteries, Optima Q. At the

Table 1
The Optima prototype batteries used in the conventional-charge and rapid-charge cycling tests. The number of cycles being tested and the total input and output ampere–hours of these batteries during the test period
Q_dis: discharge capacity; Q_chg: number of A h charged. All the batteries went through five conditioning cycles before test.

Battery I.D.	No. of cycles	Accumulated			At the end of test	
		Q_dis, A h	Q_chg, A h	Q_chg/Q_dis	Q_dis[a] (T corr'd)	Q_dis/50 A h
Conventional-charge cycled						
Optima X	51	2081	2360	1.134	56.44	1.129
Optima O	58	2300	2741	1.192	51.44	1.029
Optima V	102	4089	4421	1.081	51.21	1.024
Optima M	105	4157	5024	1.209	50.11	1.002
Optima N	237	8835	10960	1.241	40.37	0.807
Optima S	253	9701	10823	1.116	39.66	0.793
Optima Q	275	10470	12174	1.163	36.84	0.737
Rapid-charge cycled						
Optima I	73	2272	2389	1.051	48.41	0.968
Optima Z	128	4470	4707	1.053	51.56	1.031
Optima R	243	8435	8896	1.055	49.42	0.988
Optima P	909	30215	31424	1.040	45.59	0.912
Optima W	1056	34929	36542	1.046	35.58	0.712

[a] Discharge capacities with a temperature correction according to $M_c = M_r[1 - 0.009(T_c - 26.7)]$ where M_c is the temperature-corrected discharge capacity, M_r is the measured discharge capacity, and T_c is the temperature in °C.

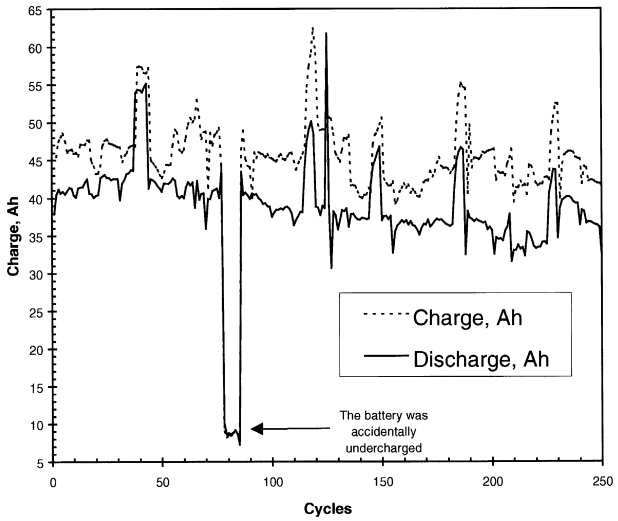

Fig. 1. Charge and discharge ampere–hours for battery Optima Q during conventional-charge cycling test.

beginning of the cycling test, a charging voltage of 15.6 V was used. The discharge capacity increased with cycling and peaked at about the 50th cycle and gradually decreased from then on. The EOC current also increased with cycling. To maintain the charging time at 10 h without excessive overcharge, as required by the test, the charging voltage was gradually reduced. At the 100th cycle, the EOC current was 0.12 A at 14.6 V. It increased to 1.0 A at the 200th cycle with the same voltage. From then on, the EOC current increased very quickly with cycling. When the test reached the 250th cycle, with the charging voltage maintained at the same level, the charge was curtailed after 4.2 h, instead of the 10 h required by the test procedure, since the charge return reached the set limit of 115%. During that period, the current was 10 A, from beginning to end. The battery failed soon after at the 275th cycle with a discharge capacity of 36.8 A h.

The cells in the failed batteries were isolated after the cycling test and were charged and discharged individually. It was found that the discharge capacities of all of the cells were limited by the negative electrodes. An example is given in Fig. 2. The figure also shows that, in the latter part of the charging period, the negative electrode was depolarised, and the EOC potential was -960 mV with respect to a Hg/Hg_2SO_4 (1.29 sp. gr. H_2SO_4) reference electrode, which was only a little more negative than the open-circuit potential of the electrode.

For comparison, the potentials of a cell in a battery, which was conditioned but not cycled, were also recorded, as shown in Fig. 3. A few facts are clearly shown. The capacity of the uncycled battery was limited by the positive electrode. The battery behaved like a flooded battery, with no obvious depolarisation occurring at the negative electrode. The EOC potential at the negative electrode was close to -1200 mV, much higher than the open-circuit potential. Since the negative electrode was not effectively

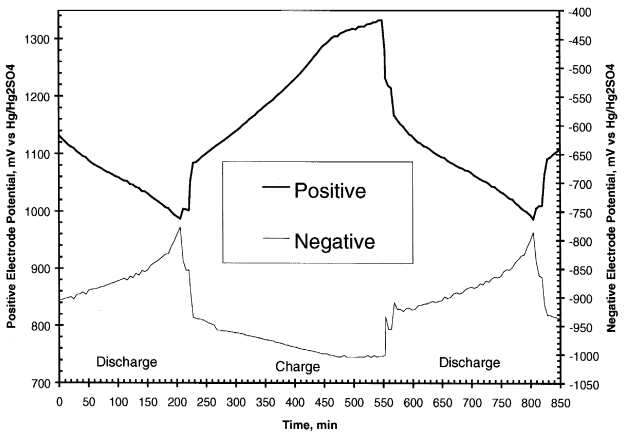

Fig. 2. Positive and negative potentials during charge and discharge in a failed test battery after 275 conventional-charge cycles (charge: 10 A, 2.35 V max; discharge: 10 A to 1.75 V).

depolarised, the positive electrode at the end of charging was only about 1260 mV, limited by the charging voltage for the cell. This was almost 100 mV lower than that in the failed battery, as shown in Fig. 2.

It was also observed that most of the failed batteries had a very high rate of self-discharge. A loss of 25% to 30% of the discharge capacity after a 3-day rest was recorded for most of the failed batteries.

Water or acid was added to the cells of the failed batteries. In most cases, no improvement in discharge capacity was recorded. However, the performance of a few cells was improved after the addition. In these cases, it was observed that the charging potential for the negative electrode was substantially raised.

3.1.2. Rapid-charge cycling

As shown in Table 1, one battery each was removed from the test at Cycles 73, 128, 243 and 909. Optima W

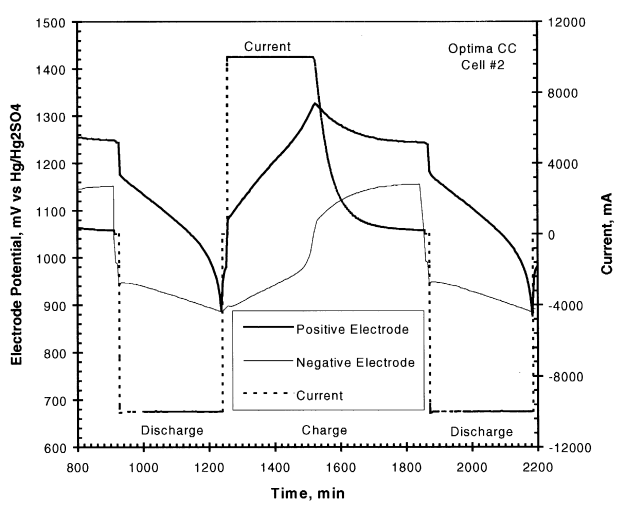

Fig. 3. Potentials of the positive and negative electrodes during charge and discharge after five conditioning cycles (charge: 10 A, 2.40 V max; discharge: 10 A to 1.75 V).

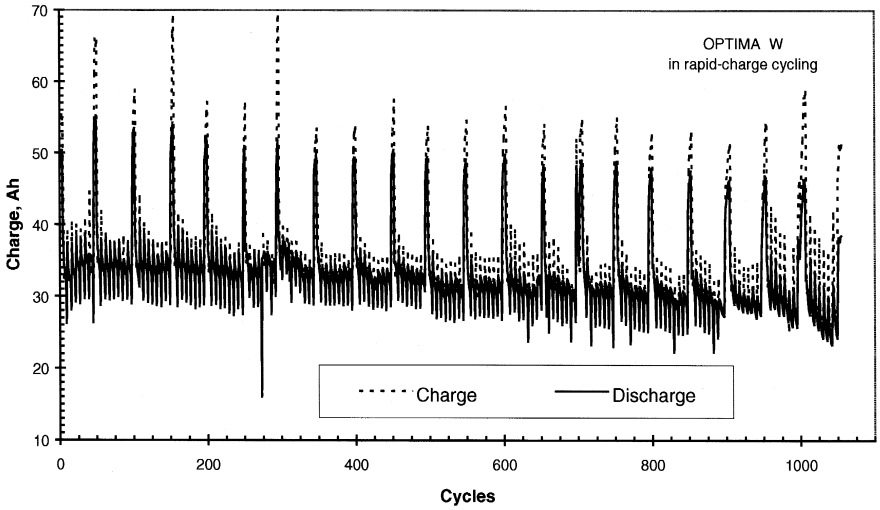

Fig. 4. Charge and discharge ampere–hours for a test battery during a rapid-charge cycling test.

was removed from the test at the 1056th cycle after it failed. Fig. 4 presents the coulombic input–output of Optima W during the test.

Fig. 5 shows details of the input–output chart of a battery during the test. In Cycles 46 to 49, the battery was capacity-discharged and then fully charged. After those cycles, the battery was cycled according to the pattern described previously: five 80% DOD discharges, each followed by a 15-min 250 A rapid charge. In the sixth cycle, the battery was charged for 4 h with a maximum current of 100 A. The experimental data revealed that, during the five partial-charge cycles, the coulombic charge efficiency was very high. For example, as shown in Fig. 5, from Cycles 51 to 55, the coulombic efficiency was 105%, 99%, 98% and 90%. The low efficiency for the fifth cycle was solely due to the experimental routine: the rest time before the discharge in the fifth cycle was 8 h (overnight), instead of 15 min as in the previous four cycles. This allowed the battery to cool down to room temperature before the discharge, instead of remaining at 40°C to 45°C as in the previous four cycles. The data also indicated that, after the 15-min charge in the fifth rapid-charge cycle, the state-of-charge of the test battery was still about 70%.

Optima W, as shown in Fig. 4, maintained its discharge capacity quite well up to about the 750th cycle, and its EOC current in the full-charge cycles (100 A maximum, 4 h) remained much smaller than 1 A. After 750 cycles, the EOC current increased with cycling, and the discharge capacity declined. For Cycles 952, 999 and 1050, at the end of the 4-h charge, the voltages were 14.6, 14.6 and 14.2 V, and the correspondent currents were 1.5, 2.8 and 3.5 A. It was also noticed that the self-discharge rate became substantial. Some of the cells of the battery were cycled after failure. The recorded potentials of the electrodes during the cycling are presented in Fig. 6. After the cell was half-charged, the positive electrode was polarised and oxygen production became substantial, which depolarised the negative electrode. Thus, the negative electrode peaked at -960 to -970 mV at half-charge, and declined to

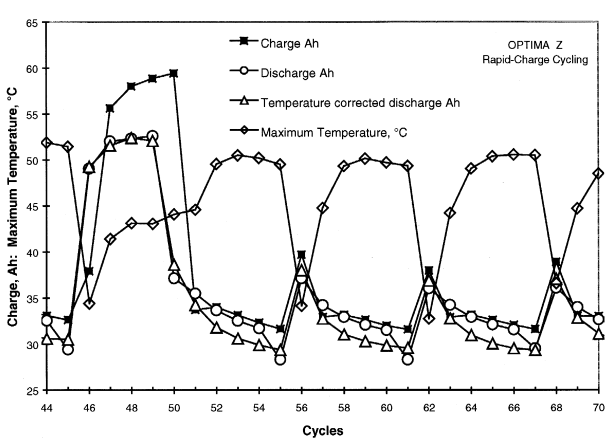

Fig. 5. Charge and discharge ampere–hours for a test battery during rapid-charge cycles (Cycles 44 to 70).

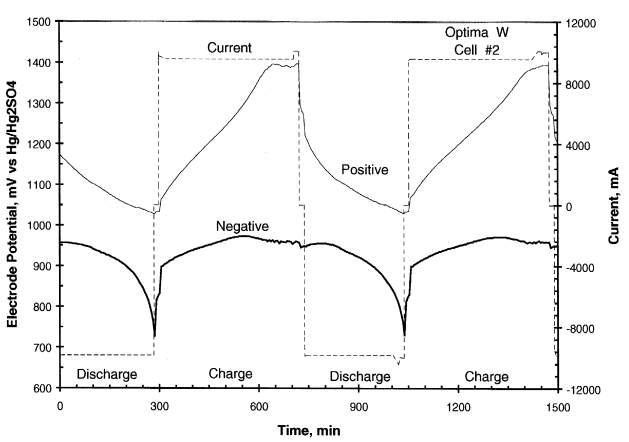

Fig. 6. Potentials of the positive and negative electrodes in a cell of a test battery during charge and discharge after its failure, after 1056 rapid-charge cycles (charge: 10 A, 2.35 V max; discharge: 10 A to 1.75 V).

Table 2
Acid concentration in separator of the test batteries in charged and discharged states

Charging method	Cycles	Acid concentration %					
		Charged			Discharged		
		Top	Middle	Bottom	Top	Middle	Bottom
Conditioned	0	41.5	41.9	42.8	14.6	8.4	17.2
Conventional	55	44.6	45.0	45.8	14.4	8.5	13.8
	103	41.1	42.6	42.2	14.2	8.8	16.7
	255 (failed)	41.1	42.0	42.2	16.2	15.3	21.8
Rapid	73	39.1	39.3	38.7	12.2	7.8	15.4
	128	41.9	42.7	43.2	11.0	6.9	18.1
	243	40.1	43.0	43.1	13.7	7.0	18.5
	909	42.2	43.0	41.9	7.5	5.0	17.3
	1056 (failed)	38.1	39.7	39.7	10.2	7.2	15.9

about -950 mV when being depolarised. Note that the charging current did not decrease with time. Even when the charge return was increased to 200%, the current still remained at 10 A, which was the set maximum.

3.2. Acid concentration

The concentrations of the acid in the separators of the test batteries were determined by titration, and the results are shown in Table 2. The data indicated that, after the conditioning cycles but before the cycling tests, when the batteries were fully charged, there was only a very small difference in concentration between the acid in the top and in the bottom of the batteries. After the batteries were discharged, the difference became larger. Most noticeable, however, was the concentration in the middle section, which became very low, at 8% (1.05 sp. gr.), after discharge. The main reason for the difference was probably that the separator was taller than the electrode and, so, protruded about 0.5 cm out of the roll of the electrodes on both ends. This provided the top and bottom sections of the electrodes with an extra reservoir of electrolyte.

This situation basically remained unchanged through the cycling test for the batteries in charged state. When the batteries were discharged, the difference between the top and the bottom appeared to be larger and the acid concentration in the middle section appeared even lower after cycling. The data in Table 2 were the average values. It was quite often that the acid in the middle section was only 3% to 4% (1.02 sp. gr.) after a full discharge.

3.3. Physical and chemical measurements of the active materials

3.3.1. Positive active material

3.3.1.1. Lead dioxide content in the positive electrode. Data are shown in Table 3 for the positive active material in the charged state. The situation appeared quite normal. The utilisation of the positive active material was less than 50% in general.

3.3.1.2. Specific surface area. The measurements are also recorded in Table 3. The surface area of the new active material (as received) had a high value of 4 to 6 m^2/g, which was substantially reduced in the conditioning cycles. It was further reduced in the ensuing cycles. The data clearly showed that the rate of reduction was much higher for conventional-charge cycling compared to that for rapid-charge cycling. They also indicated that, in conventional-charge cycling, the reduction rate was higher for the active material in the top section than that in the bottom section.

3.3.1.3. Pore-size distribution. The adsorption and desorption isotherms for all the positive active material taken from the test batteries were studied. All of them could be classified as Type II isotherms [30,31], which indicated that there was not an appreciable volume of micropores with a diameter smaller than 20 Å. The gas adsorption and desorption data were analysed using the BJH method [16,17], in which the pores were assumed to be straight and non-intersecting cylinders. The analysis showed that, for as-received active material, the distribution curve ex-

Table 3
Lead dioxide content, specific surface area, crystallite size and strain of the positive active material

Charge method	Cycles	PbO_2[a] %	α-PbO_2/β-PbO_2 wt. ratio	Surface area m^2/g			Crystallite size, μm	Crystallite strain
				Top	Middle	Bottom		
As received		72.4 (48.6)	0.95	4.33	6.31	5.49	0.024	0.00221
Conditioned	0	82.3 (55.3)	0.40	3.22	4.13	4.95	0.047	0.00171
Conventional	55	88.8 (62.5)	0.04	1.72	2.20	2.68	0.104	0.00037
	103	89.3 (62.5)	0.02	1.48	1.79	2.14	0.124	*
	255 (failed)	85.5 (70.4)	0.01	1.86	1.89	2.06	0.156	*
Rapid	73	89.5 (59.2)	0.03	2.57	2.77	2.92	0.109	*
	128	86.6 (49.6)	0.07	3.86	3.29	3.99	0.072	*
	243	86.4 (64.3)	0.02	3.78	3.33	3.98	0.118	*
	909	86.3 (61.7)	0.01	3.33	3.07	3.14	0.087	*

[a] The data in brackets are for plates which were discharged.
* Too small to be measured with certainty with the method used.

Table 4
Metallic lead content and specific surface area of the active material in the negative plates

Charge method	Cycles	Metallic Pb %	Specific surface area m^2/g			
			Top section	Middle section	Bottom section	Average
As received	–	60.8 (46.5)[a]	1.06	0.83	0.72	0.87
Conditioned	0	91.6 (57.6)	0.65	0.61	0.60	0.62
Conventional-charge cycling	55	92.3 (50.5)	0.58	0.55	0.56	0.56
	103	77.4 (59.0)	0.62	0.53	0.56	0.57
	255 (failed)	89.9 (63.9)	0.43	0.45	0.46	0.45
Rapid-charge cycling	73	80.6 (47.7)	0.57	0.59	0.57	0.58
	128	86.2 (50.1)	0.73	0.64	0.69	0.69
	243	87.6 (53.6)	0.64	0.69	0.83	0.72
	909	85.8 (53.2)	0.59	0.56	0.56	0.57
	1056 (failed)	–	0.50	0.52	0.53	0.52

[a] The data in brackets are for plates which were discharged.

hibited a peak at 160 Å and indicated an appreciable volume of pores with a diameter smaller than 150 Å. Five conditioning cycles reduced the volume of pores smaller than 150 Å by one-half, and increased that of pores with a diameter above 500 Å. In conventional-charge cycling, the volume of pores with a diameter smaller than 300 Å was reduced by one-half within 200 cycles. In contrast, the reduction rate of this portion of pores was much smaller in rapid-charge cycling and, after 1000 cycles, the volume of this portion of pores was still larger than that in conventional-charge cycling after 200 cycles.

3.3.1.4. Crystallite size and strain of β-PbO_2. As shown in Table 3, in the as-received battery, the α-PbO_2/β-PbO_2 ratio was nearly unity, which suggested that the battery was formed in a rather alkaline environment, probably due to the limited amount of acid in the battery. This ratio became smaller rapidly with cycling, more slowly in rapid-charge cycling than in conventional-charge cycling. The widths of the diffraction lines of α-PbO_2 in the as-received and conditioned active materials were large, indicating the small size of the crystallite and large strains in them. The measured size and strain for β-PbO_2 crystallites are given in Table 3. In the as-received active material, the crystallite size was 0.024 μm and the strain was 0.00221. After five conditioning cycles, the crystallite size doubled and the strain substantially reduced. The size grew with cycling, much faster in conventional-charge cycling than in rapid-charge cycling. The strain was reduced rapidly in the cycling, such that it could not be measured with any certainty using the present method after 50 cycles.

3.3.2. Negative active material

3.3.2.1. Metallic lead content. The data for both charged and discharged negative active material are given in Table 4. The data indicate that, after about 50 test cycles, the undischarged negative active material increased with cycling.

3.3.2.2. Specific surface area. Table 4 shows that the negative active material, before conditioning cycles, had a specific surface area of 1 m^2/g in the top section and 0.7 m^2/g in the bottom section, which might not have been completely formed. Five conditioning cycles reduced the surface area to 0.6 m^2/g throughout. In conventional cycling, the surface area had decreased to 0.45 m^2/g in 250 cycles, when the batteries failed. In contrast, the reduction rate was much smaller in rapid-charge cycling.

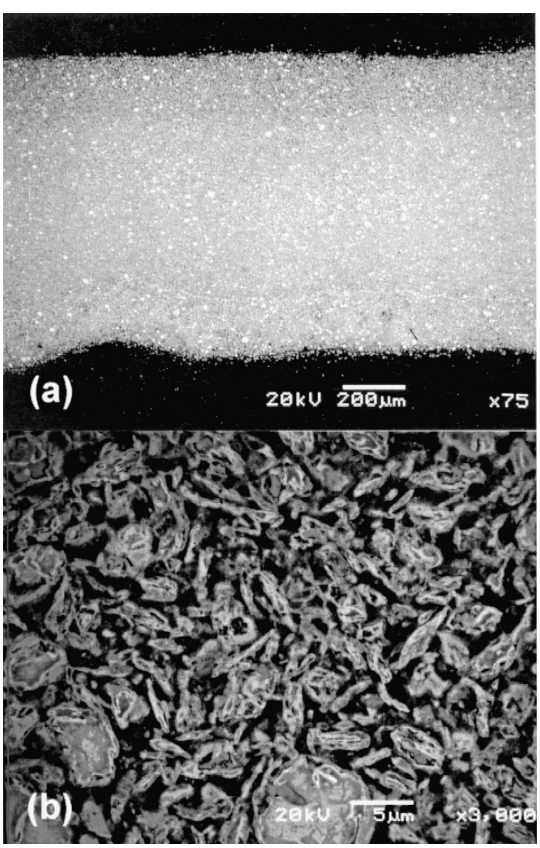

Fig. 7. The positive electrode in a test battery before cycling test (as formed). (a) Cross-section of the electrode. (b) A magnified view of the active material in the electrode.

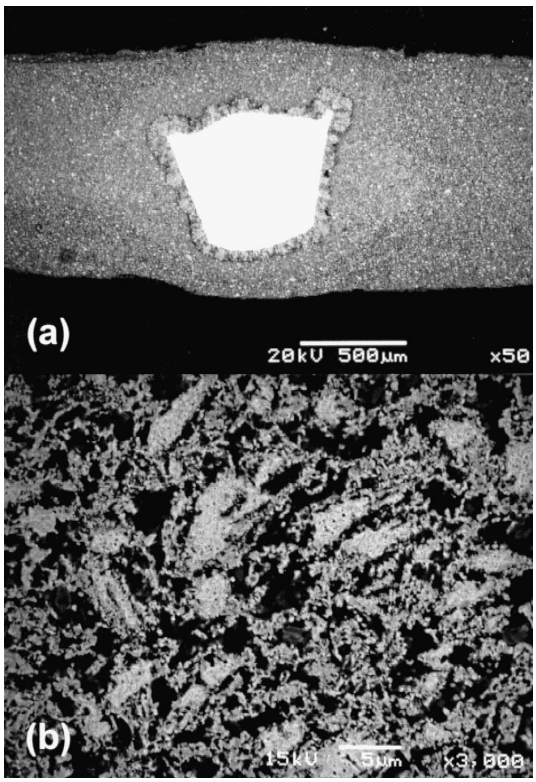

Fig. 8. Negative electrode before cycling. (a) Cross-section, including a grid wire. (b) A magnified view of the active material.

3.4. Morphology of the active materials

3.4.1. Active materials in as-received batteries

3.4.1.1. Positive active material. A cross-section of a positive plate, shown in Fig. 7a, shows that there were no visible pores at that magnification. The tiny specks dispersed in the active material were unconverted metallic lead particles. A magnified view of the active material is offered in Fig. 7b, showing numerous bar-like particles, 1 μm wide and 3 to 5 μm long, which were the products of the metasomatic conversion of tribasic lead sulfate crystals [32]. At a magnification higher than 10,000 times, submicron needle-like crystals constituting these particles could be seen (not shown in this paper).

3.4.1.2. Negative active material. A cross-section is given in Fig. 8a, showing an evenly distributed active material. There was a layer of big lead dendrites surrounding the grid member. A typical view of a high magnification of the active material is given in Fig. 8b, showing various shapes of metallic lead dendrites.

3.4.2. Active materials in conventional cycling

3.4.2.1. Positive active material. The structural change with cycling followed the process previously described by one of the authors in 1984 [32]. The bar-like particles were first hollowed out in the deep-discharge cycling after formation, creating a net-like structure which was broken down in the following cycles into evenly distributed small submicron particles. In further cycling, these dispersed particles consolidated to aggregates about 10 to 20 μm in size. With more cycling, the interparticle pores grew and the structure became coral-like. The pores then grew bigger and merged into one another. The walls of the pores became smoother. With the transformation, the activity of the active material decreased. When the big pores had permeated the whole plate, from the electrode surface to the core, the active material around the grid member started to participate in the charge–discharge process, by which it expanded and became much more porous. This allowed more acid to be available in the region. In this situation, the active material in the immediate vicinity around the grid wires, in a discharge process, would be

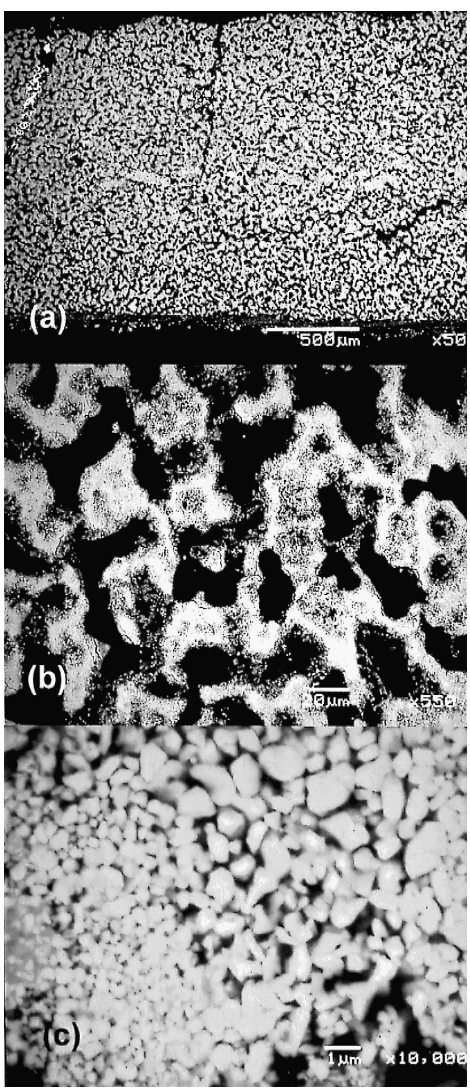

Fig. 9. Positive electrode which failed after 253 conventional-charge cycles. (a) Cross-section of a pellet of the electrode. (b) The active material close to the surface of the electrode. (c) A magnified view of the active material in a lobe of the coralloid structure shown in (b).

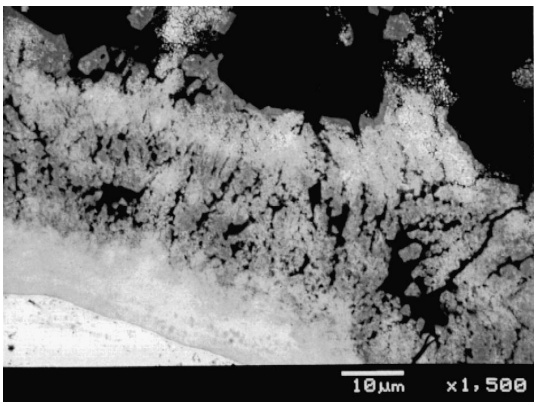

Fig. 10. A discharged portion of the grid wire/active material interface in the positive electrode after 237 conventional-charge cycles.

discharged before the active material further from the grid members had a chance to do so, and effectively would block the conductive path to the current collector. The active material in conventional-charge cycling in this investigation followed this general development path. Fig. 9a shows a cross-section of a pellet in the positive electrode after 253 conventional-charge cycles. The active material on both sides of the electrode, from the surface to a depth of one-third of the total plate thickness, was full of big pores of 20 μm and larger as shown in Fig. 9b. However, as shown by the figure, the walls of some of the smaller pores were not quite smoothed out, indicating that this portion of active material still retained some discharge capability. A magnified view of the active material in a lobe of the coralloid structure is given in Fig. 9c. Some of the lead dioxide crystals were quite big, approaching 1 μm in size. There were also crystallites so small they could not be clearly discerned even with a magnification of 10,000. The active material in the centre zone of the electrode had a coralloid structure in an early stage of development. In some batteries, the centre zone even contained thin layers of active material with net-like structure, indicating that this part of the active material had not been active in the charge–discharge cycling process. The grid wire/active material interface showed signs of substantial deterioration. It was observed that some parts of the interface, even deep in the pellet, had been participating in the charge–discharge process. As shown in Fig. 10, a portion of the grid wire was covered by a layer of lead sulfate crystals about 30 μm thick.

In summary, the morphological study revealed that the positive electrodes in the failed batteries had seriously deteriorated. However, the structure and the grid wire/ac-

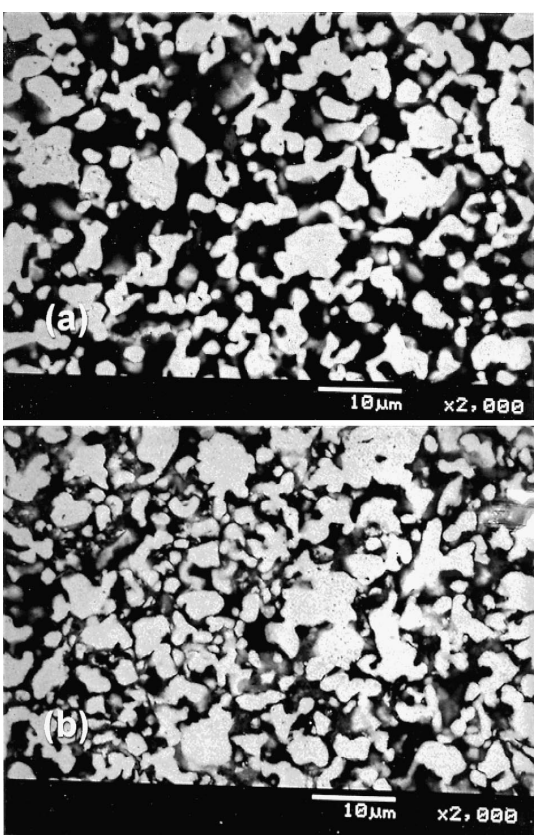

Fig. 11. Negative active material after 51 conventional-charge cycles. (a) Typical morphology of the active material. (b) The active material in the centre zone of the electrode.

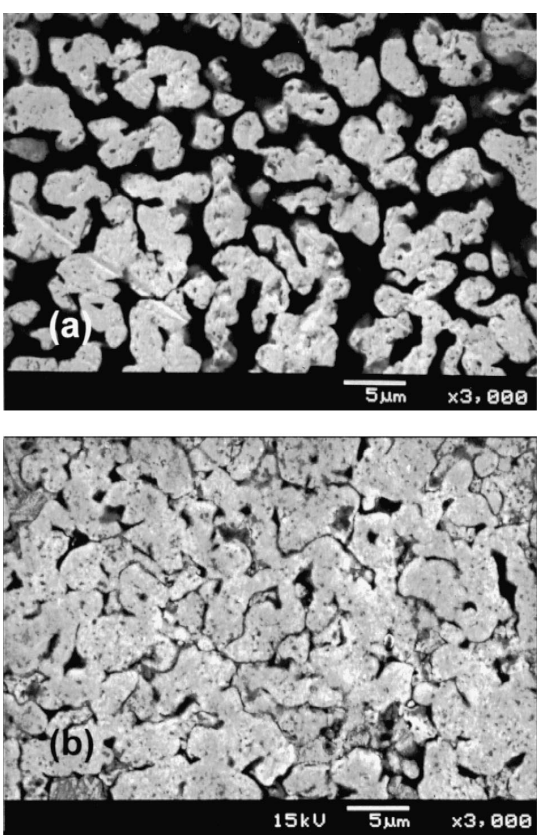

Fig. 12. Negative active material after 253 conventional-charge cycles. (a) Typical morphology. (b) The active material in the centre zone of the electrode.

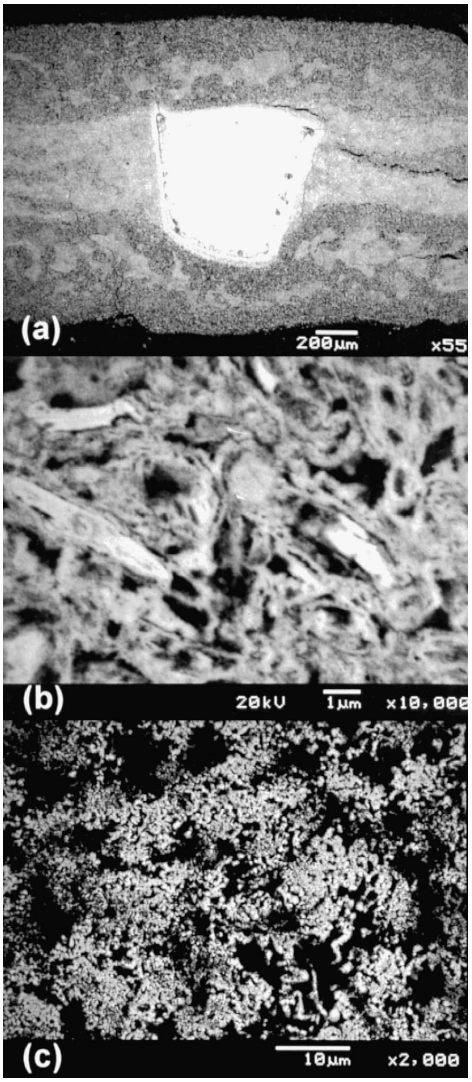

Fig. 13. Positive electrode after 243 rapid-charge cycles. (a) Cross-section, including a grid wire. (b) The active material in the dense centre layer of the electrode. (c) Formation of aggregates of the active material.

tive material interface indicated that the electrode could still sustain a few more cycles before its own failure.

3.4.2.2. Negative active material. After the formed negative electrode was cycled, the lead dendrites had broken into irregularly-shaped small lead particles of about 1 μm, as shown in Fig. 11a. It was also observed that the sponge lead was denser in the centre zone of the electrode, as shown in Fig. 11b. The lead particles grew with cycling. In the centre zone, the active material became more compacted and its utilisation decreased. When the test batteries failed at about 250 cycles, the lead particles had grown to about 3 μm, and they are, as shown in Fig. 12a, connected to one another to form a coral-like structure. The active material in the centre was so compressed, as shown in Fig. 12b, it could only be slightly utilised in the discharging process, since the compressed mass contained hardly any free space for the acid.

3.4.3. Active material in rapid-charge cycling

3.4.3.1. Positive active material. A cross-section of a portion of a positive electrode after 243 rapid-charge cycles is shown in Fig. 13a, which reveals that the active material in the centre zone, which was about one-third of the total, was much denser than the active material on both sides of it. A closer view (Fig. 13b) of the dense active material in the centre zone revealed a net-like structure, indicating that this part of the active material had not been very active in the cycling. The structure of the active material closer to the electrode surface is shown with less

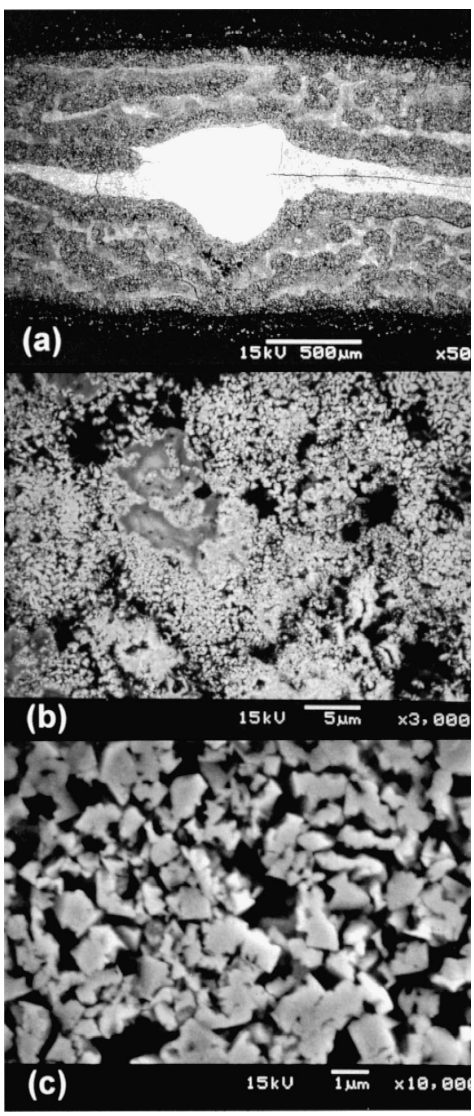

Fig. 14. Positive electrode after 1056 rapid-charge cycles. (a) Cross-section, including a grid wire. (b) Formation of aggregates of the active material. (c) A high magnified view of the active material in the aggregates.

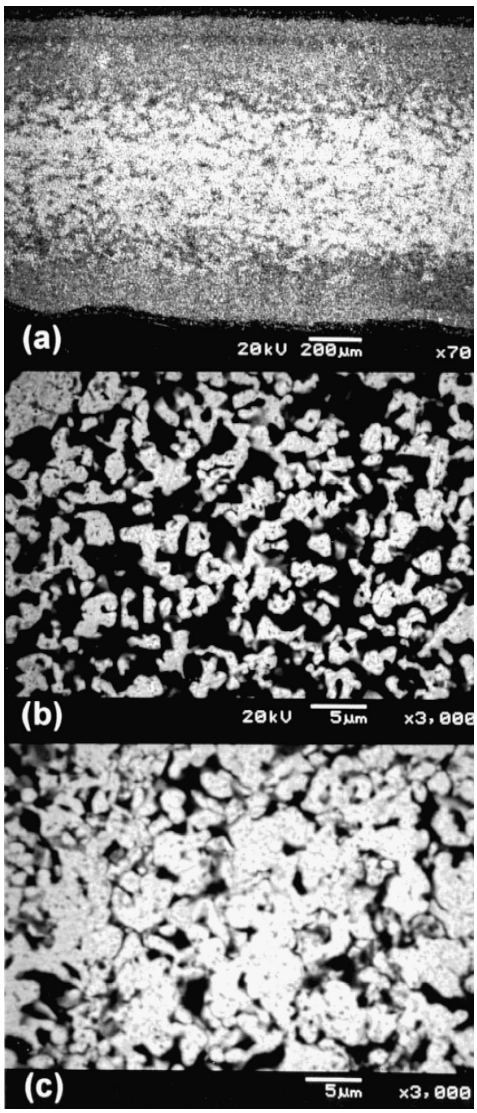

Fig. 15. Negative electrode after 243 rapid-charge cycles. (a) Cross-section. (b) Typical morphology for the active material. (c) The compacted active material in the centre zone of the electrode.

magnification in Fig. 13c. The active material here had formed aggregates of 10 to 20 μm, in which submicron lead dioxide particles were loosely packed. SEM micrographs of the discharged electrodes showed that these aggregates had reached a very high level of utilisation. In contrast, the active material in the centre zone contained hardly any lead sulfate crystals after a deep discharge.

A cross-section of a portion of the positive electrode after 1056 cycles is shown in Fig. 14a. The thickness of the dense centre zone had been reduced by cycling, compared with that after the 243 cycles shown in Fig. 13a. The structure of the active material in this centre zone was not much different from that of the as-formed active material. This layer was directly connected to the grid wires, functioning as an extension of the current collector, since it was not participating in the charge–discharge process. The active material beyond this dense central layer, as shown in Fig. 14a, was more porous, appearing as a dark substance with scattered regions of denser active material appearing as brighter strands. The dark porous active material had an aggregate structure, as shown in Fig. 14b. The lead dioxide crystals in these aggregates were similar to those in the positive electrodes subjected to conventional-charge cycling, as shown in Fig. 9c. The size of these crystals varied from submicron to about 1 μm. A more careful examination revealed that there were numerous needle-like crystals of submicron sizes. Most of them appeared to be attached to bigger crystals, as shown in Fig. 14c.

3.4.3.2. Negative active material. A cross-section of a pellet from a negative electrode after 243 rapid-charge cycles is shown in Fig. 15a. The active material closer to the surface of the electrode appeared to be porous, and that in the centre zone, much denser. Fig. 15b and c show a view of the active material in these two regions with a higher magnification. The size of the lead particles was much smaller than that in the electrode after 253 conventional-charge cycles (Fig. 12a and b). Fig. 16a and b show the active material in the porous zone close to the surface and that in the dense centre zone after 1056 rapid-charge cycles. Although the lead particles had grown with rapid-charge cycling, their size was still smaller than that in the

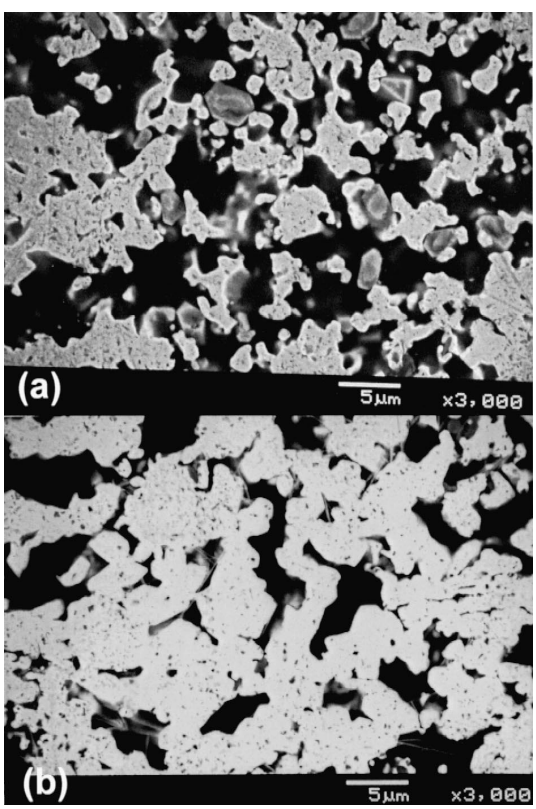

Fig. 16. Negative electrode after 1056 rapid-charge cycles. (a) Typical morphology for the active material. (b) The compacted active material in the centre zone of the electrode.

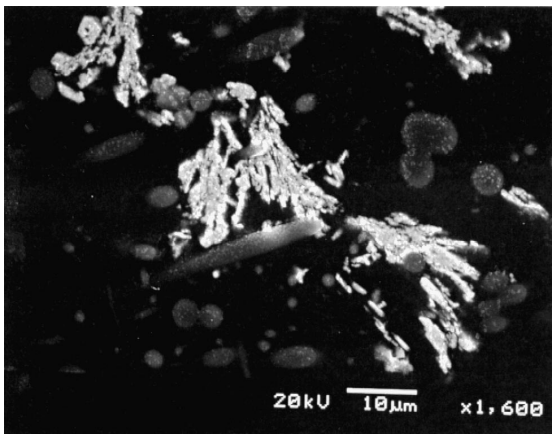

Fig. 17. Lead dendrites in the separator of a failed battery after 1056 rapid-charge cycles.

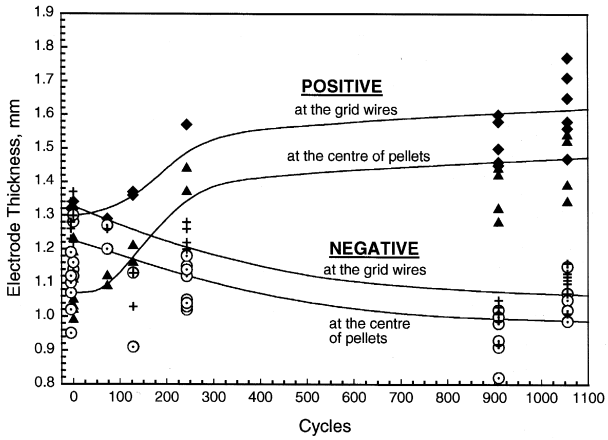

Fig. 19. Change in the thickness of the positive and negative electrodes in rapid-charge cycling.

negative electrodes that had been through only about 250 conventional-charge cycles. Only a small amount of lead sulfate had been found in the dense centre zone when the battery was discharged, indicating that the active material there did not contribute much to the discharge capacity of the negative electrodes.

3.4.3.3. Separator. No pin-holes through the separator caused by lead dendrites were found in any of the failed batteries. However, there were numerous lead sulfate crystals in the separators of the batteries in every stage of the cycling test. Lead dendrites were found in the separator of failed batteries with a high self-discharge rate, as shown in Fig. 17.

3.4.4. Thickness of the electrodes

The thickness of the electrodes was measured from the SEM images. The thickness of an electrode was measured at two locations: at the spot where a grid wire was and at the centre of a pellet. Figs. 18 and 19 show the variation of the electrodes in conventional-charge and rapid-charge cycling, respectively. In conventional-charge cycling, the positive electrode expanded quickly in the first 100 cycles. After that, there was very little further growth. At the failure point, about 250 cycles, the average growth at the grid wire was 23%, and that at the centre of a pellet was 55%. Meanwhile, the negative electrodes shrank. There was a reduction of 24% at the centre of the pellets when the batteries failed.

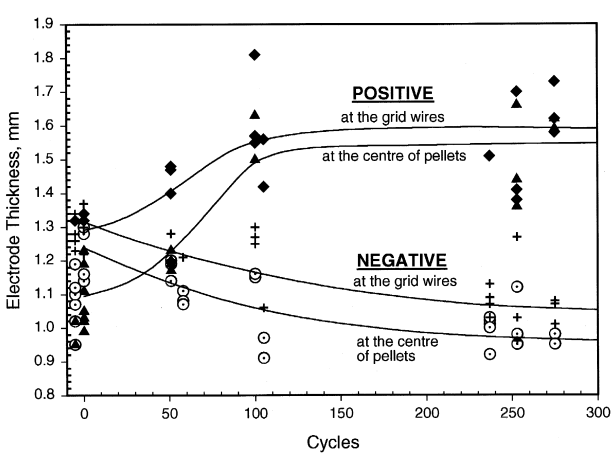

Fig. 18. Change in the thickness of the positive and negative electrodes in conventional-charge cycling.

In comparison, the expansion of the positive electrode and the shrinkage of the negative electrode in rapid-charge cycling proceeded at a much slower pace, compared with those in conventional-charge cycling. The largest difference is in the growth of the pellets of the positive active material. The average thickness of the pellet centres in the positive electrodes, after 1000 rapid-charge cycles, was 1.4 mm, but 1.55 mm after only 250 conventional-charge cycles.

4. Discussion

4.1. Morphological changes of positive active material with cycling

4.1.1. Lead dioxide crystallites

In the as-received electrode, the amount of α-PbO_2 was about the same as that of β-PbO_2 (Table 3). It decreased quickly with cycling. The rate of decrease in conventional-charge cycling was much higher than that in rapid-charge cycling. This actually mainly indicated that the positive electrodes in rapid-charge cycling had more unused active material being preserved in the central part of the electrode. There was a measurable strain in both α and β forms of lead dioxide in the as-received electrode (Table 3). After 50 cycles, α-PbO_2 practically disappeared, and the strain in β-PbO_2 declined from 0.002 to less than 0.0004, to a level at which it could not be reliably measured with our equipment. The average size of the lead

dioxide in the as-received batteries was 0.024 μm (Table 3). It doubled after the five conditioning cycles. It grew larger in conventional-charge cycling, reaching 0.16 μm when the batteries failed at about 250 cycles. In rapid-charge cycling, the average size grew to about 0.1 μm after 73 cycles. The experimental data indicated that the average size was kept at this level for up to 900 rapid-charge cycles. The unused active material in the centre zone of the electrode certainly kept the value down in the rapid-charge cycling. However, after reaching 900 cycles, the amount of the preserved unused active material was relatively small. Thus, the data suggested that the size of the crystallites produced by rapid charging was relatively small. This is supported by the observation of the submicron needle-like crystallites (Fig. 14c).

4.1.2. Positive active material structure

In as-received (as-formed) batteries, the positive active material was mainly the result of metasomatic transformation from tribasic lead sulfate crystals. When a battery was conventional-charge cycled, the structure transformation of the active material followed the classical evolution path [32]. With cycling, a network structure formed first. The active material appeared as quite evenly distributed submicron lead dioxide particles after the network structure was destroyed. Aggregates, 10 to 20 μm large, soon formed on further cycling. They then consolidated into a coralloid structure. In this stage, the activity of the active material decreased. With more cycling, the pores grew bigger and the walls of the pores grew smoother. The structural integrity became poorer as the pores grew large, which eventually led to disintegration. The rate of transformation was not uniform in the electrode. It first occurred in the active material close to the surface and then worked its way inward. After 50 conventional-charge cycles, the coralloid structure became the major structure. After 100 cycles, a considerable amount of big pores had formed. When the batteries failed at about 250 conventional-charge cycles, the big pores were prevalent and they encircled the grid wires. In contrast, the active material in rapid-charge cycling did not develop into a coralloid structure. The development was arrested in the aggregate (agglomeration) stage. In this stage, the distribution of pore size was nearly ideal, with a good combination of micro-pores and macro-pores [32]. As a result, the active material in this development stage had a high utilisation. Since the part of the active material which participated in the charge–discharge process deteriorated only very slowly with rapid-charge cycling, the amount of unused active material in the centre of the pellets also entered the cycling process very slowly. Thus, throughout their cycle lives, the positive electrodes in rapid-charge cycling always had a dense and highly conductive layer in the centre of the pellets, acting as an extension of the current collector.

As the structure of the active material changed with cycling, the volume of the active material became larger, especially with the formation of a coralloid and big-pore structure. At the end of life in conventional-charge cycling, the average expansion at the centre of the pellets was 55%. In comparison, the expansion was much slower in rapid-charge cycling. The expansion exerted an additional pressure on the negative material.

4.2. Morphological changes of negative active material with cycling

When the as-formed negative active material was cycled, the lead dendrites were destroyed to form interconnected small lead particles. With cycling, the particles grew and the surface area of the active material decreased. The growth rate was much higher in conventional-charge cycling. At the end of their cycle life, at about 250 cycles, the lead particles grew from 3 to 5 μm, with smooth rounded corners and surfaces. The specific surface area decreased to 0.45 m^2/g (Table 4). This led to a loss of activity of the active material. In comparison, the growth of lead particles and the loss of surface area were much slower in rapid-charge cycling. After 900 cycles, the specific surface area was measured at 0.53 m^2/g, and the SEM examination showed that there were still a substantial number of particles of about 1 μm in size.

The loss of discharge capacity in cycling was not only caused by growth of the lead particles. The morphological study using SEM showed very clearly that the metallic lead in the centre zone of the electrode was being compressed during the cycling. When the batteries failed after 250 conventional-charge cycles, the lead particles in the centre portion of the electrode, about one-third of the total mass, were compressed into a dense mass with small pore volume, and, subsequently, a very small discharge capacity. At the beginning of the cycling, the capacities of the batteries were limited by the positive electrode (Fig. 3). Therefore, after a discharge, most of the negative active material would still be in the form of metallic lead. Due to better accessibility to the acid, the active material closer to the surface of the electrode would have greater of being converted to lead sulfate than that in the interior of the electrode. The active material, which was constantly being charged and discharged, was much less compressible than that which always stayed in metallic form because of the existence of sulfate crystals in the pores of the cycled portion. In the test batteries, the spirally-wound positive and negative electrodes were tightly packed in strong cylindrical cells which did not allow any expansion of the electrode assembly. In this situation, an expansion of the positive electrode would immediately cause a compression of the negative electrode. The positive electrode in conventional-charge cycling expanded much faster with cycling than in rapid-charge cycling. Thus, the negative electrode suffered more compression from the expansion of the positive electrode in the conventional-charge cycling. Figs. 18 and 19 show that the degree of compression suffered by

the negative electrode after 250 conventional-charge cycles was equivalent to that after 1000 rapid-charge cycles.

If a battery failed due to the low activity of the negative electrode which was brought about by the compression of the negative active material, a design to add more negative active material into the battery to compensate the loss of its capacity might not be very effective, since the densification rate for the negative active material would be higher, when the ratio of negative to positive active material was raised.

4.3. Cause of failure of the test batteries

The post-mortem study, as presented in the previous discussion, clearly showed that the failure of the test batteries was brought about by the loss of discharge capacity of the negative electrode. However, the positive electrode of the failed batteries in conventional-charge cycling tests deteriorated to such a degree that it would have failed soon in further cycling, if that had been conducted. In the case of rapid-charge cycling tests, the positive electrode still had retained an appreciable cycling capability at the point of battery failure.

At the point of failure, the negative active material was seriously deteriorated. However, this was not the immediate cause of failure in most of the cases. The failing batteries usually exhibited a high EOC current, an excessively high self-discharge rate, and an EOC negative potential that was low and close to the equilibrium value. These facts suggest that there were internal shorts in the failed batteries.

Okada [33] found what he called "soak-through" shorting in failed batteries. He reported that, if a lead-acid cell was allowed to be discharged to the extent that acid concentration fell to a very low level, especially to the stage when the polarities of the electrodes were reversed, or if the cell was allowed to stand in water or very dilute acid, a recharge would result in internal shorting. The separator would then contain metallic lead particles and other lead compounds. Although he found metallic particles and a white deposit in the separator, he had observed no "pin-hole" shorts. He argued that a lead compound precipitated in the separator first and, subsequently, the charging of the battery reduced the lead compound to metallic lead and caused "soak-through" shorting. His description agreed with our observations. Our data showed that, after a discharge, the measured acid concentration in the separator could be as low as 2% (1.012 sp. gr.). Lead sulfate has a higher solubility in acid of low concentrations [34,35]. After the battery was charged, the concentration was back to 1.3 to 1.31 sp. gr., in which the solubility of lead sulfate was drastically reduced. In the discharged state, if the solution was saturated with lead sulfate, in the subsequent charging, the solution would become oversaturated and a deposition of lead sulfate in the separator could occur. With a considerable build-up of lead sulfate in the separator, some part of the sulfate deposit would be converted to metallic lead (Fig. 17) during a charging period, forming many tiny conducting paths through the separator.

In the previous discussion, it was shown that there was a big expansion of the positive electrode in the cycling test, which may have been the cause of the densification of the negative active material. The data also showed that the negative electrode might not be very compressible in the place where grid wires were located. Therefore, inevitably, there would be numerous locations where the separator was greatly compressed instead. These numerous short paths between the two electrodes would accelerate the establishment of shorts. Thus, the expansion of the positive electrode not only compressed the negative electrode and caused densification of the negative active material, but also compressed the separator and encouraged the formation of minute shorts through the separator.

4.4. Overcharge factor

In the conventional-charge cycling test, the batteries were overcharged every cycle. In the rapid-charge cycling test, besides being overcharged in the three capacity-discharge cycles after every 50 test cycles, the battery also got an overcharge in the 4-h full charge after every five rapid-charge cycles. However, in the five consecutive rapid-charge cycles (Fig. 5), the batteries were undercharged, although the overcharge factor was close to unity in the last three cycles of the five-cycle pattern. Thus, in the rapid-charge cycling test, when the battery failed after 1000 cycles, it had been subjected to over 250 cycles in which the battery was substantially overcharged, quite comparable to the number in conventional-charge cycles.

Table 1 showed that, for the three batteries which were cycled to failure in the conventional-charge cycling test, the overcharge factors ranged from 1.12 to 1.24, all higher than the average overcharge factor of 1.05 for those in the rapid-charge cycling test. The variation of the overcharge factor for the three batteries (Optima N, S and Q) actually reflected the mode of failure of the batteries. The average overcharge factor was high (1.24) for Optima N because, after 100 test cycles, the "soak-through" shorts started to develop, which caused the EOC current to rise, resulting in a higher overcharge factor. Optima S failed mainly because of the deterioration of the negative active material, the enlargement of the lead particles, and the densification of the lead in the centre core. With a much smaller EOC current, the overcharge factor of Optima S was, therefore, much smaller than that of Optima N, and closer to the average value for the 250 full charges received by the batteries (Optima P and W) in the rapid-charge cycling test. This analysis suggests that the difference in the overall overcharge factors for the batteries was not the

critical factor responsible for the much better performance given by the batteries in rapid-charge cycling: a longer cycle life by a factor of 4 and a much larger total discharge output during the cycle life by a factor of 3.

5. Summary and conclusion

When spirally-wound valve-regulated lead-acid batteries, using absorptive glass mat as separators, were subjected to conventional-charge and rapid-charge cycling, the following was observed.

(1) The batteries subjected to rapid-charge cycling, compared with those subjected to conventional-charge cycling, exhibited a longer cycle life by a factor of 4 and a larger total ampere-hours output by a factor of 3.

(2) The discharge capacity of the batteries was limited by the positive electrode when the cycling tests started, but was limited by the negative electrode when the batteries failed, regardless of which charging regime was used.

(3) In conventional-charge cycling, the structural change of the positive active material followed a general path of evolution, in which the formation and development of a coralloid structure is the last stage. In this stage, the active material expands markedly and loses its discharge capacity and integrity quickly. The active material in conventional-charge cycling started to develop a coralloid structure after 50 cycles. In contrast, in rapid-charge cycling, the active material did not develop into that stage and was arrested at the stage of aggregates, in which the active material enjoyed high utilisation and much less expansion.

(4) There is evidence that submicron needle-like lead dioxide crystals were produced in rapid charging which enhanced the utilisation of the active material.

(5) The lead particles of the negative active material in rapid-charge cycling grew at a much slower rate.

(6) In the cycling tests, the expansion of the positive active material caused a compression of the negative active material. After 250 conventional-charge cycles, the active material in the centre zone, one-third of the total mass, was compressed into a dense lead mass with a very low porosity, which was almost totally inactive. This process occurred in the rapid-charge cycling at a much slower pace.

(7) The immediate cause of failure for most of the batteries was the occurrence of "soak-through" shorting. Since the amount of acid in the valve-regulated batteries was limited, a drastic fluctuation of acid concentration occurred during cycling. This caused lead sulfate to deposit in the separator and, consequently, the formation of lead dendrites through the separator. It was possible that the expansion of the positive active material also compressed the separator, creating many short paths between the electrodes that encouraged the development of shorts.

Acknowledgements

This investigation was supported by the Advanced Lead-Acid Battery Consortium, Research Triangle Park, NC, USA. Dr. P.T. Moseley's initiation and proposal of the measurements of the crystallite size and strain, using X-ray diffractometry, are gratefully acknowledged.

References

[1] J.L. Woodbridge, Trans. Am. Inst. Electr. Eng. 54 (1935) 516.
[2] G.W. Vinal, Storage Batteries, 4th edn., Wiley, New York, 1935, p. 244.
[3] H. Bode, Lead-Acid Batteries, Wiley, New York, 1977, p. 308.
[4] D.E. Gosden, J. Power Sources 45 (1995) 61.
[5] E.M. Valeriote, J.K. Nor, V.A. Ettel, Very fast charging of lead-acid batteries, Proc. 5th Int. Lead/Acid Battery Seminar, International Lead Zinc Research Organization (ILZRO), Research Triangle Park, NC, 1991, p. 93.
[6] J.K. Nor, Proc. 25th Internat. Symposium on Automotive Technology, Florence, Italy, June 1–5, 1991.
[7] E.M. Valeriote, D.M. Jochim, J. Power Sources 40 (1992) 93.
[8] T.G. Chang, E.M. Valeriote, D.M. Jochim, Comparative Fast Charging of Lead-Acid Batteries, Proc. 26th Int. Symposium on Automotive Technology, Aachen, Germany, September 13–17, 1993, pp. 405–413.
[9] T.G. Chang, E.M. Valeriote, D.M. Jochim, J. Power Sources 48 (1994) 163.
[10] T.G. Chang, D.M. Jochim, J. Power Sources 64 (1997) 103.
[11] J.K. Nor, European Patent 0 311 460 A2, October 10, 1988; U.S. Patent 5,202,617, April 13, 1993.
[12] J.K. Nor, Proc. 25th Internat. Symposium on Automotive Technology, Florence, Italy, June 1–5, 1991.
[13] J.K. Nor, Proc. 11th Int. Electric Vehicle Symposium, Florence, Italy, September 27–30, 1992, Paper No. 9.03.
[14] J.K. Nor, Proc. 26th Int. Symposium on Automotive Technology, Aachen, Germany, September 13–17, 1993, Paper 93EL020, p. 375.
[15] J.K. Nor, D.R. Smith, Very Fast Battery Charging and Battery Energy Management, Proceedings of the 12th International Electric Vehicle Symposium, Anaheim, California, December, 1994.
[16] E.P. Barrett, L.S. Joyner, P.P. Halenda, J. Am. Chem. Soc. 73 (1951) 373.
[17] S.J. Gregg, K.S.W. Sing, Adsorption, Surface Area and Porosity, 2nd edn., Academic, London, 1982.
[18] H.P. Klug, L.E. Alexander, X-ray Diffraction Procedures for Polycrystalline and Amorphous Materials, 2nd edn., Wiley, New York, 1974.
[19] D. Balzar, J. Appl. Crystallogr. 25 (1992) 559.
[20] D. Balzar, H. Ledbetter, J. Appl. Crystallogr. 26 (1993) 97.
[21] D. Balzar, J. Res. Natl. Inst. Stand. Technol. 98 (1993) 321.
[22] D. Balzar, H. Ledbetter, J. Mater. Sci. Lett. 11 (1992) 1419.
[23] D. Balzar, H. Ledbetter, A. Roshko, Powder Diffr. 8 (1993) 2.
[24] J.I. Langford, Accuracy in Powder Diffraction II, NIST Special Publication 846, US Government Printing Office, Washington, D.C., 1992, p.110.
[25] Th.H. De Keijser, J.I. Langford, E.J. Mettemeijer, A.B.P. Vogels, J. Appl. Crystallogr. 15 (1982) 308.
[26] Th.H. De Keijser, E.J. Mittemeijer, H.C.F. Rozendaal, J. Appl. Crystallogr. 16 (1983) 309.
[27] B.E. Warren, X-ray Diffraction, Addison Wesley, Reading, MA, 1969.
[28] N.H. Furman, Standard Methods of Chemical Analysis, The Elements, Vol. I, 6th edn., p. 578.

[29] D.H. Collins (Ed.), Batteries, MacMillan, New York, 1963, p. 439.
[30] S.J. Gregg, K.S.W. Sing, Adsorption, Surface Area and Porosity, 2nd edn., Academic Press, Toronto, 1982.
[31] S. Lowell, J.E. Shields, Powder Surface Area and Porosity, 3rd edn., Chapman and Hall, London, 1991.
[32] T.G. Chang, J. Electrochem. Soc. 131 (1984) 1755.
[33] K. Okada, Yuasa Jiho 81 (1996) 3.
[34] E.M. Valeriote, L.D. Gallop, P.J. Aragon, Can. J. Chem. 57 (1979) 974.
[35] V. Danel, V. Plichon, Electrochim. Acta 27 (1981) 771.